ISSN 1063-7826, Semiconductors, 2009, Vol. 43, No. 11, pp. 1420–1427. © Pleiades Publishing, Ltd., 2009.
Original Russian Text © S.G. Dorofeev, N.N. Kononov, A.A. Ishchenko, R.B. Vasil'ev, M.A. Goldschtrakh, K.V. Zaitseva, V.V. Koltashev, V.G. Plotnichenko, O.V. Tikhonevich, 2009, published in Fizika i Tekhnika Poluprovodnikov, 2009, Vol. 43, No. 11, pp. 1460–1467.

SEMICONDUCTOR STRUCTURES, INTERFACES, AND SURFACES

Optical and Structural Properties of Thin Films Precipitated from the Sol of Silicon Nanoparticles

S. G. Dorofeev[a], N. N. Kononov[b]^, A. A. Ishchenko[c], R. B. Vasil'ev[d], M. A. Goldschtrakh[c], K. V. Zaitseva[c], V. V. Koltashev[e], V. G. Plotnichenko[e], and O. V. Tikhonevich[b]

[a] *Department of Chemistry, Moscow State University, Moscow, 119991 Russia*
[b] *Prokhorov Institute of General Physics, Russian Academy of Sciences, Moscow, 119991 Russia*
^*e-mail: nnk@kapella.gpi.ru*
[c] *Lomonosov State Academy of Fine Chemical Technology, Moscow, 119571 Russia*
[d] *Department of Material Sciences, Moscow State University, Moscow, 119991 Russia*
[e] *Research Center of Fiber Optics, Russian Academy of Sciences, Moscow, 119333 Russia*

Submitted March 26, 2009; accepted for publication April 6, 2009

Abstract—A new technique of growing nanocrytalline silicon (*nc*-Si) thin films is suggested. The technique involves the centrifuge-assisted size-selective deposition of nanoparticles from a colloidal solution (sol) containing *nc*-Si powders. The structural and optical parameters of the initial *nc*-Si powders and films deposited by the newly suggested procedure are studied by transmission electron microscopy and analysis of absorption spectra and Raman spectra. The absorption coefficient of the *nc*-Si films increases with decreasing dimensions of the constituent nanoparticles. The experimentally measured band gap of the films, E_g, is widened from 1.8 to 2.2. eV on etching the *nc*-Si powders used for deposition of the corresponding films. On the basis of the analysis of the Raman spectra, it is suggested that the amorphous component is involved in the *nc*-Si powders and films due to oxygen atoms arranged at the nanoparticle surface.

PACS numbers: 68.55.-a, 68.60.-p, 81.07.Wx, 81.15.-z

DOI: 10.1134/S1063782609110050

1. INTRODUCTION

Thin nanocrystalline silicon (*nc*-Si) films offer considerable promise as elements of solar cells [1], thin-film transistors [2, 3], gas sensors, and single-electron devices [4, 5]. The prospects of the *nc*-Si films for use in solar cells are caused by the fact that the fundamental absorption edge of such films can be shifted to photon energies lower than 1 eV that are beyond the region of absorption of single-crystal silicon (*c*-Si). In addition, such films do not exhibit the effect of light-induced degradation (Staebler–Wronski effect) observed in hydrogenated amorphous silicon (*a*-Si:H). When used in thin-film transistors, the *nc*-Si films show a high mobility of charge carriers and high electrical stability [2, 3].

At the present time, there are several technologies of deposition of thin (~100 nm) *nc*-Si films. Among the technologies, the most often used method is the plasma enhanced chemical vapor deposition (PECVD) of the films from silane (SiH_4) at low pressures.

In this paper, we describe a new method of fabrication of thin *nc*-Si films. The method involves the fractional deposition of nanoparticles onto the substrate by centrifuging their sol in ethanol. We present data on transformation of the size distribution of particles in the *nc*-Si powders, when treated (etched) in the solutions of hydrofluoric acid HF and its mixture with the nitric acid, HF + HNO_3. The results of comparative analysis of the absorption spectra of the films produced from the initial *nc*-Si powders and the powders subjected to etching are described. The results of spectral studies suggest that, in contrast to *c*-Si, the *nc*-Si films produced here exhibit noticeable absorption at photon energies up to ~0.6 eV below the fundamental absorption's edge. It is shown that, as the nanoparticle dimensions are reduced, surface states attributable to hydrogen and oxygen atoms located at the nanoparticle surface begin to make a noticeable contribution to the optical characteristics of the films.

We report the results of comparative analysis of the absorption spectra and Raman spectra for the films produced from the initial *nc*-Si powders and the corresponding spectra for films produced from the powders subjected to etching. We show that, in the films deposited from the etched *nc*-Si powders, absorption in the range of incident photon energies 1.0 eV $\le \hbar\omega \le$ 3 eV is controlled basically by electron states related to the nanoparticle surface.

It is found that the *nc*-Si powders and the films deposited from these powders involve an amorphous component, whose relative content varies during etching and deposition of the particles onto the substrate.

From the analysis of Raman spectra, we conclude that this amorphous component is associated with oxygen atoms that are located at the nanoparticle surface and distort the nanoparticle crystal lattice.

2. EXPERIMENTAL

2.1. Synthesis of Powders and Deposition of nc-Si Films

The system for synthesis of the *nc*-Si powders and conditions of the process are described in detail elsewhere [6, 7]. In what follows, we briefly outline the procedure of synthesis of the Si nanoparticles. In a reactor chamber filled with a buffer gas (helium or argon) to the pressure $P = 200$ Torr, a fine SiH_4 jet is formed and heated by focused cw CO_2 laser radiation beam crossing the jet. During pyrolysis of silane, the SiH_4 molecules are decomposed, and free Si atoms are produced. When colliding with each other and with the atoms of the buffer gas, the Si atoms form particles, whose average dimensions can be in the range from 10 to 100 nm, depending on the pressure of the buffer gas.

The *nc*-Si powders produced in such a manner were dispersed by ultrasonic treatment in ethanol and centrifuged for 30 min with an acceleration of 2000*g* (*g* is the gravitational acceleration). As a result, almost all agglomerates of *nc*-Si particles are precipitated. After preliminary centrifugation, a stable colloidal solution (sol) of *nc*-Si in ethanol remains. No visible changes in the solution, including precipitations, were observed for two years. For the subsequent deposition of nanoparticles, a water solution of aluminum dihydrophosphate was added to the sol.

To etch the nanopaticles, we added a portion of the *nc*-Si colloidal solution to the aqueous solution of the $HF + HNO_3$ mixture or to the solution of the HF acid and then subjected the resulting mixtures to ultrasonic treatment for different times, in accordance with the concentration of acids. To stop etching in the solution of the $HF + HNO_3$ acids, we added a tenfold volume of water to the reaction mixture. Etching of the particles in the solution of HF stopped spontaneously because of passivation of the nanoparticle surface. As a result of etching, the particles lost their capability of forming a sol. To restore the solvability, we washed the nanoparticles with distillated water in an ultrasonic bath three times, with the intermediate separation of the particles from washing solutions by centrifuging for 10 min with the acceleration 2000*g*. In this case, we obtained the *nc*-Si sols that do not precipitate in the centrifuge.

To fabricate films, we subjected the substrate with the sol, coagulated aluminum hydrophosphate, to centrifuging, after which the *nc*-Si film was deposited onto the substrate surface. The *nc*-Si films were deposited at the first, second, and third stages of centrifugation of the sols. In this case, it was assumed that the film formed in each succeeding stage of size-selective deposition consisting of particles smaller in size. The thickness of the *nc*-Si films deposited in such a manner in the study was varied from 40 nm to 2 μm. To increase the mechanical strength, we annealed the *nc*-Si films in vacuum (at the pressure 10^{-5} Torr) at temperatures from 423 to 673 K.

2.2. Methods of Analysis

The shape and size distribution of particles in the initial *nc*-Si powders and the powders subjected to etching were studied by transmission electron microscopy (TEM) with the use of a LEO912AB OMEGA microscope. The size distribution of the *nc*-Si particles was determined by processing the TEM images with the use of the UTH SCSA Image Tool program. The thickness of the *nc*-Si films was determined with a Taly Step (Taylor-Hobbson) profilometer. The transmittance spectra of the films in the ultraviolet (UV) and visible spectral regions were recorded with the use of a Lambda 900 (Perkin Elmer) spectrophotometer.

The Raman spectra of the films were recorded with a microlens-equipped T-64000 (Jobin Ivon) Raman triple spectrograph in the backscattering layout of measurements at the power of the excitation argon laser 2 mW.

3. RESULTS AND DISCUSSION

3.1. TEM Analysis

According to the TEM data, the shape of particles in the initial *nc*-Si powder is nearly spherical, and the particles themselves coagulate to form agglomerates up to several hundreds of nanometers in dimensions. The peak of the size distribution of the particles in the initial *nc*-Si powders corresponds to the diameter $L(nc\text{-Si})_{max} \approx 20$ nm.

Figure 1 exemplifies the size distribution of the *nc*-Si particles, as obtained from the computer-assisted analysis of the TEM images. Etching of the *nc*-Si powder in the aqueous solution of acids (5 wt % HF + 14 wt % HNO_3) shifts the peak of the size distribution to $L(nc\text{-Si})_{max} \approx 3$ nm, and etching in the water solution of HF at the concentration of 12 wt % to $L(nc\text{-Si})_{max} = 7–13$ nm. From the comparison of histograms shown in Figs. 1a and 1b, it can be seen that, for the powder etched in the ($HF + HNO_3$) mixture, the size distribution of the *nc*-Si particles exhibits a single well-pronounced maximum. For the powder etched in the solution of HF, we observe a more complex structure of the size distribution. This feature of the size distribution of the *nc*-Si particles treated with the HF acid can be associated with the stop of etching that is finished, when the surface of the *nc*-Si particle gets saturated with hydrogen. In addition, since the surface of such particles is free of oxide envelopes, the rate of coagulation is larger, and as a result, large-sized agglomerates are formed.

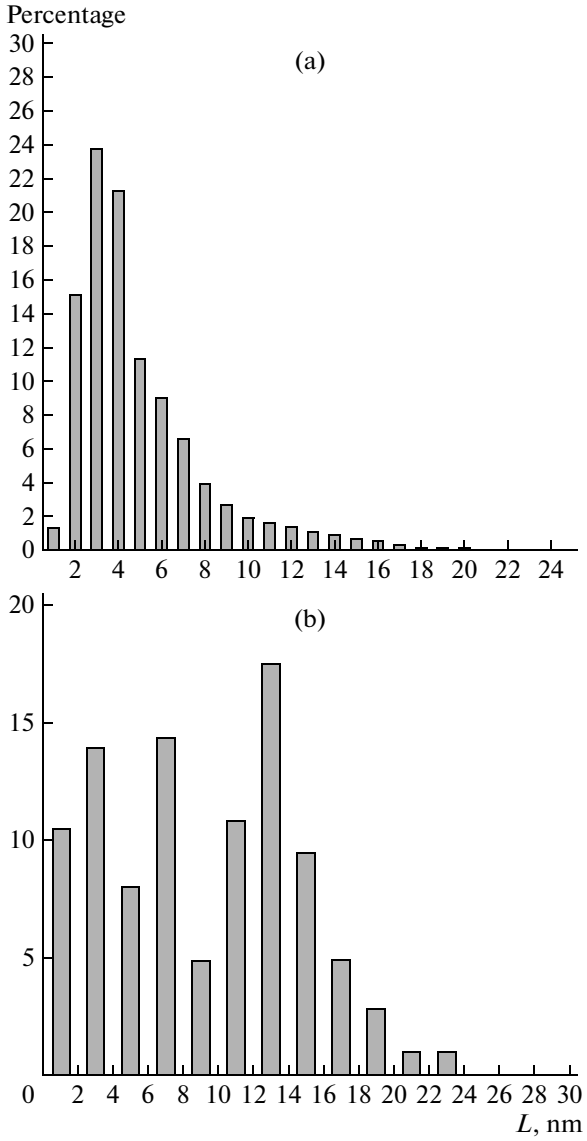

Fig. 1. (a) Histogram of the size distribution of particles, as obtained by processing of the TEM images of the *nc*-Si powder etched in the (HF + HNO_3) acid mixture (see table). (b) Histogram of the size distribution of particles, as obtained by processing of the TEM images of the *nc*-Si powder etched in the HF acid (see the table).

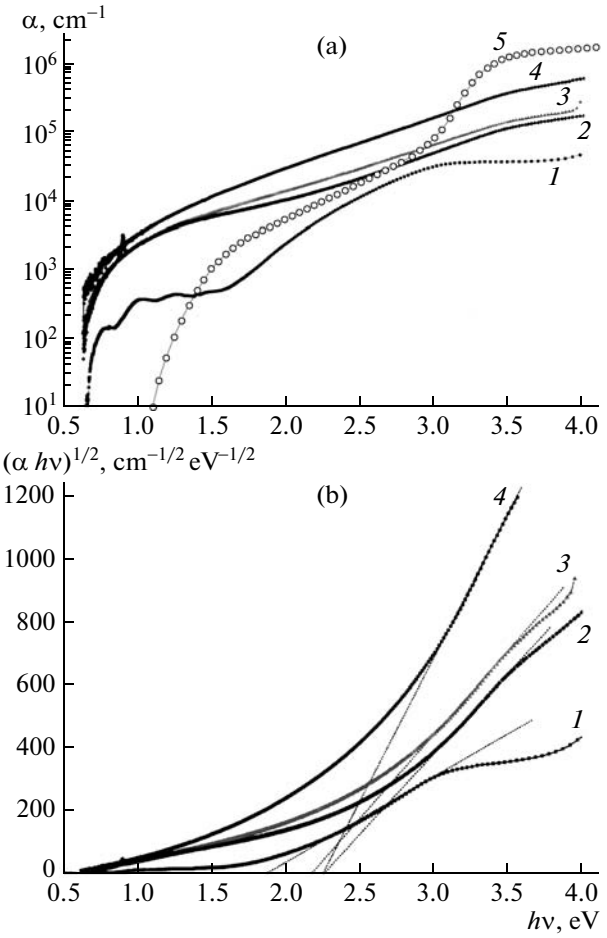

Fig. 2. (a) Optical absorption spectra of films (curves *1*–*4*) (see the table). Open circles refer to the absorption spectrum of single-crystal silicon. (b) Optical absorption spectra of films (curves *1*–*4*) (see table) in the coordinates $\sqrt{\alpha\hbar\omega}$ –$\hbar\omega$. Dotted lines correspond to the dependences $\sqrt{\alpha\hbar\omega} = A(\hbar\omega - E_g)$ for the films.

3.2. UV and Visible Absorption

To record the transmittance spectra, we deposited the *nc*-Si particles from the sols onto quartz substrates. For comparative analysis, we recorded the transmittance spectra of the films deposited from the *nc*-Si sols at the first, second, and third stages of size-selective deposition. The notation of the films produced from the sol of the initial *nc*-Si powder is given in the table.

From the transmittance spectra, we calculated the absorption coefficients of the films. The dependences of the absorption coefficients on the incident photon's energy are shown in Fig. 2a. Figure 2a shows also the absorption spectrum of *c*-Si for comparison.

From the absorption spectra shown in Fig. 2a, it is evident that, all of the films studied here (see the table) noticeably absorb radiation in the range of incident photon energies 0.6 eV ≤ $\hbar\omega$ ≤ 1.0 eV. This feature makes the spectra of the films radically different from the absorption spectrum of *c*-Si.

The second significant feature of the spectra of the films is the fact that the absorption coefficients of films *2* and *3* are higher than the absorption coefficient of *c*-Si also in the range of incident photon energies 1.0 eV ≤ $h\omega$ ≤ 3.0 eV. Such behavior of the absorption coefficient of microcrystalline Si films was observed also in [8–10]; however, the physical cause of such behavior was not established. In the case of the films produced in this study, the high absorption coefficients in the above-indicated energy region are rather unex-

pected. In fact, from the TEM data for the *nc*-Si powders, from which the films were deposited, we can see that the dimensions of a significant portion of particles in these powders are smaller than 10 nm. Consequently, taking this fact into account, we can conclude that the absorption coefficient of such films is bound to depend on the increase in the band gap due to the effect of quantum confinement. It is obvious that such an increase in the band gap is bound to yield a decrease in the absorption coefficient at any incident photon energy (a blue shift of the absorption band). The blue shift is actually observed for films *2* and *3* at the energies $\hbar\omega \geq 2.7$ eV and for film *4* at $\hbar\omega \geq 3.1$ eV, i.e., near the critical point corresponding to the direct $\Gamma'_{25}-\Gamma_{15}$ transition in *c*-Si.

The effect of quantum confinement on the optical properties of the films can be detected by analyzing the energy dependences of $\sqrt{\alpha\hbar\omega}$, where $\alpha(\hbar\omega)$ is the absorption coefficient at the photon energy $\hbar\omega$. These dependences for films *1*–*4* are plotted in Fig. 2b. From the plots, it can be seen that, for film *1* at the range of incident photon energies $2.2\ \text{eV} \leq \hbar\omega \leq 3.0$ eV and for films *2, 3*, and *4* at the incident photon energies $3.0\ \text{eV} \leq \hbar\omega \leq 3.5$ eV, the function $\sqrt{\alpha\hbar\omega}$ can be adequately fit by the linear dependence $\sqrt{\alpha\hbar\omega} = A(\hbar\omega - E_g)$. In accordance with Tauc's model [11, 12] when applied to amorphous silicon, the quantity E_g found from such dependence defines the band gap in *a*-Si:H. A similar procedure of data processing was applied to the data for porous silicon (*p*-Si) [13, 14], and the linear extrapolation $\sqrt{\alpha\hbar\omega} = A(\hbar\omega - E_g)$ in the vicinity of the critical points corresponding to the fundamental transition $\Gamma'_{25}-X_1$ and the indirect transition $\Gamma'_{25}-L_1$ in the absorption spectrum yielded $E_g = 1.80$ and 2.50 eV, respectively. For *c*-Si at room temperature, $E_g(\Gamma'_{25}-X_1) = 1.12$ eV and $E_g(\Gamma'_{25}-L_1) = 1.80$ eV [15]; therefore, the authors of [13] thought of the larger values of E_g [13] as resulting from the increase in the fundamental $\Gamma'_{25}-X_1$ band gap and the indirect $\Gamma'_{25}-L_1$ band gap in *p*-Si due to quantum confinement.

In films *1, 3*, and *2* and *4* (see the table), the band gap E_g is, correspondingly, 1.80, 2.20, 2.25 eV (Fig. 2b), noticeably larger than the fundamental band gap of *c*-Si. Since the energy region, in which the above linear approximation is valid, is in the vicinity of the critical point $\Gamma'_{25}-L_1$, we relate the experimentally determined quantities E_g with the band gap at this point in the films. As noted above, for *c*-Si, $E_g(\Gamma'_{25}-L_1) = 1.80$ eV; therefore, we can state that, for film *1*, no effect of quantum confinement is observed. At the same time, for films *2, 3*, and *4*, the quantum confinement increases the indirect $E_g(\Gamma'_{25}-L_1)$ band gap by 0.40 and 0.45 eV, respectively.

Identification of films produced from the sol of the initial nc-Si powder

Film number	Effect of acids[a]	nc-Si film thickness, nm[b]	Stage of selective deposition of fractions
1	No etching	1600	1
2	5 wt % HF + 14 wt % HNO_3	215	2
3	12 wt % HF	180	2
4	12 wt % HF	45	3

Notes: [a] The duration of the reaction with acids is 1 h at the temperature 293 K.
[b] The accuracy of the step profilometer Taly Step (Taylor-Hobbson) used in the measurements corresponds to 2 nm. However, the roughness of the film surface and the irregularities of the film thickness increase the relative error to ~15%.

From the comparison of the absorption coefficients of films *2, 3*, and *4* in the range of incident photon energies $1.0\ \text{eV} \leq \hbar\omega \leq 3.0$ eV, it can be seen that the most significant absorption is inherent in the thinnest film (film *4*), whose thickness is 45 nm. The absorption spectrum of film 4 is very similar to the spectrum of film *3* deposited from the same sol of *nc*-Si at the preliminary stage of centrifuging. From Fig. 1b, it can be seen that the size distribution of the *nc*-Si particles etched in the solution of HF (12 wt %) exhibits several peaks. It can be naturally suggested that the *nc*-Si particles deposited from the sol at the preliminary stage of centrifuging are bigger than the particles deposited at the next stage. Correspondingly, it seems rather probable that film *4* is formed of smaller *nc*-Si particles than film *3*. Since the average particle's dimensions in both films *3* and *4* do not exceed 10 nm, the properties of such particles are bound to depend to a noticeable extent on electron states associated with the particle surface. The effect of surface states is enhanced with reducing particle dimensions, and since film *4* is formed of particles smaller than those of film *3*, the effect of surface states on the absorption in film *4* is bound to be more pronounced than the corresponding effect in film *3*. Thus, the absorption spectra of films *3* and *4* give us grounds to state that, in the range of photon energies $1.0\ \text{eV} \leq \hbar\omega \leq 3.0$ eV, the absorption is controlled basically by electron states associated with the Si nanoparticle's surface. This conclusion is applicable also to film *2* formed of the sol of *nc*-Si etched in the (HF + HNO_3) mixture. In fact, as follows from the above consideration, the band gap in film *2* is the same as in film *4* (see also Fig. 2b). Therefore, it can be believed that the average nanoparticles dimensions in films *2* and *4* are close and, since the specific surface areas in films *2* and *4* are close, the effects of surface states on the absorption are bound to be nearly identical as well. However, from Fig. 2a, we

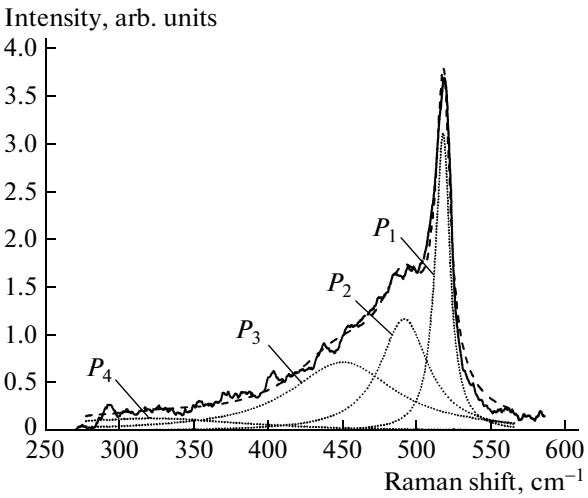

Fig. 3. Raman spectrum of film S_3 deposited from the sol of the *nc*-Si powder etched in the ($HF + HNO_3$) acid mixture (see the table for film 2). The dotted line refers to the approximation of the spectrum with Lorentzian contours (the P_1, P_2, P_3, and P_4 peaks).

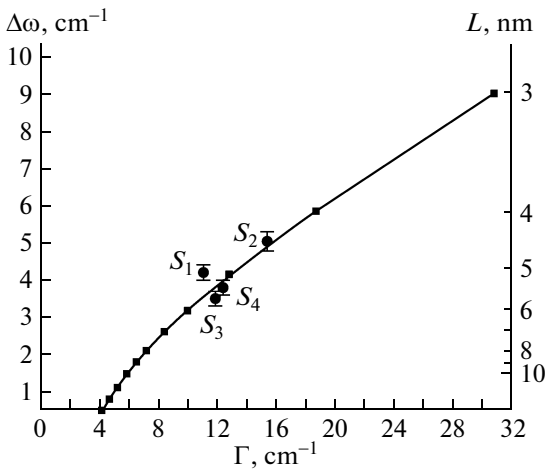

Fig. 4. The half-width and the red shift of the P_1 Raman peak versus the diameter of the spherical silicon nanoparticles, as obtained (solid line) in the context of the phonon's confinement model [19, 20] and (solid circles) from the approximation of the P_1 peak in samples S_1, S_2, S_3, and S_4 with the Lorentzian contours.

can see that, in the region of incident photon energies $\hbar\omega \geq 1.5$ eV, the absorption coefficient of film *4* is nearly three times larger than the absorption coefficient of film *3*. This difference apparently arises from the different conditions of passivation of the Si nanoparticle's surface, when etched in the solution of the only HF acid and when etched in the ($HF + HNO_3$) mixture. The difference between the absorption coefficients of films *2* and *4* suggests that the concentration of electron states associated with the *nc*-Si particle surfaces in films *2* differs from the concentration of such states in film *4* and that these states can be different in nature. The difference in the character of surface states is bound to be controlled by the relationship between the concentrations of the (≡Si–H) and (≡Si–O–) fragments at the nanoparticle surface, and this relationship depends on the history of treatment of the surface.

3.3. Raman Scattering

To record the Raman spectra, we first deposited an aluminum film with the thickness ~300 μm onto the quartz substrate, and then, on top of the film, we deposited the *nc*-Si film from the sol. We proceeded in such manner in order to avoid the background scattering component produced by the quartz substrate.

In Subsection 3.3, we analyze the Raman spectra recorded for the initial *nc*-Si powder, for the films deposited at the second stage of centrifuging the sols of the initial *nc*-Si powder and the powder etched in the ($NF + HNO_3$) mixture in the conditions corresponding to film *2* (see the table), and for the film similar to film *2* but annealed for 1 h in vacuum at the pressure $P = 10^{-5}$ Torr and the temperature $T = 673$ K. The corresponding samples are identified as samples S_1, S_2, S_3, and S_4, respectively. The typical Raman spectrum recorded for film S_3 is shown in Fig. 3. All of the experimentally recorded spectra are very similar to the Raman spectra obtained for *p*-Si in [16, 17] and for the *nc*-Si clusters in [18]. The Raman spectra of all of the samples studied here can be fitted with four Lorentzian bands with a rather good accuracy (Fig. 3). In what follows, these bands are referred to as the P_1, P_2, P_3, and P_4 peaks.

The Raman shift of the most intense P_1 peak with respect to the emission frequency of the probing laser is in the range of wave numbers from 515 to 517 cm^{-1} for all of the samples. The Raman shift of the similar peak for *c*-Si corresponds to the wave number 520.5 cm^{-1}. Thus, for all of the films studied here, the P_1 peak is shifted to smaller wave numbers with respect to the peak for *c*-Si (the red shift).

The P_1 peak in the Raman spectra of the *nc*-Si particles is due to light scattering assisted by longitudinal optical (LO) and transverse optical (TO) phonons at the central point Γ'_{25} of the Brillouin zone for the *c*-Si crystal lattice. The red shift of the P_1 peak and its half-width as functions of the nanoparticle dimensions are adequately described in the context of the phonon's confinement model [19, 20]. The result of application of this model to spherical nanoparticles is shown in Fig. 4. From Fig. 4, it can be seen that the average dimension of the *nc*-Si particles in the samples is in the range 4–6 nm, irrespective of whether the particles of the initial *nc*-Si powder were subjected to some treatment or not. For the sols of the *nc*-Si powders etched in the ($HF + HNO_3$) mixture, the average particle's dimensions determined in the phonon's confinement

model are in good agreement with the particle dimensions corresponding to the peak of size distribution obtained for the particles by processing of the TEM images. However, for the initial *nc*-Si powders, the average particle dimensions determined by the above-mentioned two methods differ by a factor of about 3.

There are two possible causes of the difference between the average particle's dimensions determined in the phonon's confinement model and by processing of the TEM images.

One of the causes is associated with the fact that, in the phonon's confinement model, the nanoparticles are assumed to be single crystals. Therefore, the magnitude of the phonon wave's vector q in the nanoparticle can vary in the range $(0, 2\pi/L)$, where L is the particle diameter. However, if the nanoparticle core is polycrystalline and the average dimension of the elementary crystal lattice in the core is l, the confining condition $q \le 2\pi/L$ should be replaced by the condition $q \le 2\pi/l$. Thus, it is possible that the dimensions $l = 4$–6 nm calculated in the phonon's confinement model are related to the average dimensions of elementary lattices in the polycrystalline nanoparticle cores rather than to the average nanoparticles' dimensions in the initial *nc*-Si powder. From this assumption and the fact that, for nanoparticles subjected to etching, the average dimensions determined by the above two methods are the same, it follows that, on such etching of the nanoparticles, the remaining *c*-Si cores are single crystals.

The other cause can follow from the well-known low contrast of the finest nanoparticles (with the diameter 3 nm in the case under study) in the TEM images. Because of the low contrast, the processing of the TEM images always reduces the relative portion of the fine-grained fraction of nanoparticles in the ensemble of particles under consideration.

The Raman shift of the P_2 peak in the samples is in the range from 480 to 495 cm^{-1}. This peak corresponds to the TO-phonon-assisted scattering in *a*-Si:H. Similarly to the P_2 peak, the P_3 and P_4 peaks are related to the amorphous component of the structure of the Si particles and result from scattering assisted by LO and longitudinal acoustic (LA) phonons.

From the comparison of the integrated intensities of the P_1 and P_2 peaks, I_c and I_a, we can determine the volume fraction of the crystalline phase, X_c, in the Si particles. To do this, we used the expression [21] $X_c = \dfrac{I_c}{I_c + \eta I_a}$, where $\eta = \dfrac{\sigma_c}{\sigma_a}$ is the ratio between the integrated backscattering's cross sections in the crystalline and amorphous fractions (corresponding to the P_1 and P_2 peaks). According to [22], the quantity η for silicon is $\eta = 0.8$–0.9. In the calculations, we set $\eta = 0.8$. For samples S_1, S_2, S_3, and S_4, the values of the parameter X_c are 0.45, 0.35, 0.50, and 0.60, respectively. From these values of X_c, it follows that almost a half of the volume of the particles is characterized by a high degree of disorder of the crystal lattice.

From comparison of the above values, it is evident that, in film S_2 deposited at the second stage of centrifuging from the sol with the initial *nc*-Si powder, the parameter X_c is smaller than X_c for the initial powder. The average particle's dimension in film S_2 is smaller than that in the initial powder. Correspondingly, the surface area to volume ratio for the particles in the S_2 film is larger than the corresponding ratio in the initial powder. Therefore, the effect of the nanoparticle surface on the general properties of the nanoparticles in film S_2 is bound to be more pronounced that the corresponding effect in the initial powder. Consequently, the smaller value of X_c (the higher degree of amorphization of the particles) in film S_2 in comparison with X_c in sample S_1 suggests that the disordered region is at the nanoparticle surface rather than in the nanoparticle core. However, for films S_3 and S_4, the value of X_c is larger than X_c for film S_2, although the average particle's dimensions in these films are comparable. Such difference suggests that the degree of disorder of particle surfaces in films S_3 and S_4 is lower than that in film S_2.

Since films S_3 and S_4 are deposited from the sols of the *nc*-Si powders subjected to etching, such lower degree of disorder in these films is due to the effect of the HF and HNO_3 acids on the particle surface. Here, it is reasonable to mention the studies [23, 24], in which the effect of oxygen atoms on the structure of silicon clusters and on the degree of ordering of the Si crystal lattice in nanoparticles is analyzed, and the studies [17, 25], in which the changes induced in the Raman peak similar to the P_2 peak (Fig. 3) by the effect of oxygen on the surface of *p*-Si passivated with hydrogen, are reported. The general idea of the above-mentioned studies is that the crystal lattice of nanoparticles, whose surface is completely passivated with hydrogen, is practically the same as the lattice of the silicon crystal. However, if oxygen atoms appear at the nanoparticle surface, they can form the Si–O–Si and (Si=O) bonds and, thus, distort the lattice at the distances up to 0.5 nm. In this space region, the distortions of angles between the Si–Si bonds in the crystal lattice can be as large as 10° [17]. Therefore, if the surface of a nanoparticle of a diameter smaller than 3 nm is coated with the SiO_2 oxide, the crystal lattice is distorted within a noticeable volume fraction of such particle. As a consequence, if the *p*-Si surface is etched in the solution of HF, the Raman spectrum involves only one peak similar to the P_1 peak. If *p*-Si is exposed to oxygen in oxygen-containing atmosphere, the Raman spectrum exhibits also the P_2 peak along with the P_1 peak. From the above-mentioned studies and from the analysis of the Raman spectra discussed here, we can make the statement presented below. At the surface of *nc*-Si nanoparticles in all samples, there is a noticeable number of oxygen atoms, which distort the crystal lattice in these particles and bring about the appearance

of the P_2 peak in the Raman spectra. Since the average nanoparticle's dimensions in film S_2 are smaller than those in powder S_1, the effect of these oxygen atoms on the crystal lattice structure in film S_2 is more pronounced than the effect in powder S_1. As a result, the volume fraction of the crystal phase in film S_2 is reduced compared to that in S_1.

Etching of the *nc*-Si particles in the solution of the (HF + HNO_3) acids results in a decrease in the particle dimensions. However, in this case, the total number of oxygen atoms at the nanoparticle's surface decreases, since a portion of oxygen atoms is replaced with hydrogen atoms. Therefore, in films S_3 and S_4, two opposite processes are bound to occur. One process related to the decrease in the nanoparticle's dimensions yields a decrease in X_c, whereas the other process related to the decrease in the number of oxygen atoms at the nanoparticle surface brings about an increase in X_c. In films S_3 and S_4, we experimentally observe the parameter X_c larger than X_c in film S_2; therefore, we can conclude that, on etching of the *nc*-Si particles, the latter process dominates over the former one.

The larger value of X_c in film S_4 compared to X_c in film S_3 suggests that, on vacuum annealing at the pressure $P = 10^{-5}$ Torr and temperature $T = 673$ K, a considerable portion of oxygen atoms leaves the nanoparticle surface.

4. CONCLUSIONS

The results of spectral measurements show that the films studied here exhibit noticeable absorption in the energy region extended to the energies ~0.6 eV below the fundamental absorption edge of crystalline silicon.

The size distribution of nanoparticles is determined from the TEM images for the initial *nc*-Si powders and the powders subjected to etching. It is established that, after etching in the solution of HF, the size distribution of particles is described by an unsteadily varying function characterized by several peaks. At the same time, after etching in the (HF + HNO_3) mixture, the size distribution of particles exhibits only one peak, as observed for the initial powder (Fig. 1).

By processing the absorption spectra, the band gap of the films E_g is calculated. From the comparison of E_g with the corresponding parameter of *c*-Si, it is found that, in the films deposited from the sols of the *nc*-Si powders a priori treated in the solutions of the (HF + HNO_3) acids, the indirect band gap $\Gamma'_{25} - L_1$ is wider because of the effect of quantum confinement.

It is found that the smaller the average dimensions of the constituent particles in the film, the larger the absorption coefficient of the film, all other factors being the same. It is shown that, at smaller nanoparticle dimensions, a more significant contribution to the optical characteristics of the film is made by surface states that can be associated with the hydrogen and oxygen atoms at the nanoparticle surface.

From the Raman spectra, it follows that, in the initial *nc*-Si powders and in the films deposited from the sols of these powders, there is an amorphous component. The relative content of such component changes on etching of the *nc*-Si powders and on deposition of films from the sols with such powders.

From the comparison of the relative content of the crystalline component in the films deposited from the sols of the initial *nc*-Si powders with the content in the films produced from the etched powders, it is established that the crystal lattice is distorted in the regions near the nanoparticle surface. The most probable factor responsible for distortions of the crystal lattice near the nanoparticle surface is the oxygen atoms arranged at the surface.

ACKNOWLEDGMENTS

This study was supported by the Russian Foundation for Basic Research, project no. 07-02-00955-a.

REFERENCES

1. A. Shan, E. Vallat-Shauvain, P. Torres, J. Meier, U. Kroll, C. Hof, C. Droz, M. Goerlitzer, N. Wyrsch, and M. Vanechek, Mater. Sci. Eng. B **69–70**, 219 (2000).
2. J.-C. Cheng, S. Allen, and S. Wagner, J. Non-Cryst. Sol. **338–340**, 720 (2004).
3. C. H. Lee, A. Sazonov, and A. Nathan, Appl. Phys. Lett. **86**, 222106 (2005).
4. S. Tiwari, F. Rana, C. Chan, L. Shi, and H. Hamafi, Appl. Phys. Lett. **69**, 1232 (1996).
5. R. Tsu, Appl. Phys. A **71**, 391 (2000).
6. G. P. Kuz'min, M. E. Karasev, E. M. Khokhlov, N. N. Kononov, S. B. Korovin, V. G. Plotnichenko, S. N. Polyakov, V. I. Pustovoy, and O. V. Tikhonevich, Laser Phys. **10**, 939 (2000).
7. N. N. Kononov, G. P. Kuz'min, A. N. Orlov, A. A. Surkov, and O. V. Tikhonevich, Fiz. Tekh. Poluprovodn. **39**, 868 (2005) [Semiconductors **39**, 835 (2005)].
8. H. Richter and L. Ley, J. Appl. Phys. **52**, 7281 (1981).
9. W. B. Jackson, N. M. Johnson, and D. K. Bigelsen, Appl. Phys. Lett. **43**, 195 (1983).
10. A. Poruba, A. Feifar, Z. Remeŝ, J. Ŝpringer, M. Vaneček, J. Kočka, J. Meier, P. Torres, and A. Shah, J. Appl. Phys. **88**, 148 (2000).
11. J. Tauc, R. Grigorovici, and A. Vancu, Phys. Stat. Solidi **15**, 627 (1966).
12. S. K. O'Leary and P. K. Lim, Solid Commun. **104**, 17 (1997).
13. M. Ben-Chorin, B. Averboukh, D. Kovalev, G. Polisski, and F. Koch, Phys. Rev. Lett. **77**, 763 (1996).
14. D. Kovalev, G. Polisski, M. Ben-Chorin, J. Diener, and F. Koch, J. Appl. Phys. **80**, 5978 (1996).
15. R. A. Forman, W. R. Thurber, and D. E. Aspens, Solid State Commun. **14**, 1007 (1974).

16. R. Tsu, H. Shen, and M. Dutta, Appl. Phys. Lett. **60**, 112 (1992).

17. J. C. Tsang, M. A. Tischler, and R. T. Collins, Appl. Phys. Lett. **60**, 2279 (1992).

18. M. Ehbrecht, H. Ferkel, F. Huisken, L. Holz, Yu. N. Polivanov, V. V. Smirnov, O. M. Stelmakh, and R. Schmidt, J. Appl. Phys. **78**, 5302 (1995).

19. H. Richter, Z. Wang, and L. Ley, Solid State Commun. **39**, 625 (1981).

20. I. H. Campbell and P. M. Faushet, Solid State Commun. **58**, 739 (1986).

21. A. T. Voutsas, M. K. Hatalis, J. Boyce, and A. Chiang, J. Appl. Phys. **78**, 6999 (1995).

22. H. Kakinuma, M. Mohri, M. Sakamoto, and T. Tsuruoka, J. Appl. Phys. **70**, 7374 (1991).

23. A. Puzder, A. J. Williamson, J. C. Grossman, and G. Galli, Phys. Rev. Lett. **88**, 097401 (2002).

24. M. Luppi and S. Ossicini, Phys. Rev. B **71**, 035340 (2005).

25. Ma Zhixun, Liao Xianbo, Kong Guanglin, and Chu Junhao, Sci. China A **43**, 414 (2000).

Translated by É. Smorgonskaya